Exciton saturation in GaAs multiple quantum wells at room temperature

Exciton saturation in GaAs multiple quantum wells at room temperature

A. Miller, P. Riblet, M. Mazilu, S. White, T. M. Holden et al.

Citation: J. Appl. Phys. **86**, 3734 (1999); doi: 10.1063/1.371244
View online: http://dx.doi.org/10.1063/1.371244
View Table of Contents: http://jap.aip.org/resource/1/JAPIAU/v86/i7
Published by the American Institute of Physics.

Exciton saturation in GaAs multiple quantum wells at room temperature

A. Miller,[a] P. Riblet, M. Mazilu, S. White, T. M. Holden, A. R. Cameron, and P. Perozzo
School of Physics and Astronomy, University of St Andrews, Fife, KY16 9SS, Scotland, United Kingdom

(Received 16 March 1999; accepted for publication 30 June 1999)

Pump-probe experiments in GaAs/AlGaAs multiple quantum well samples are described using both picosecond and femtosecond laser pulses in different polarization configurations. The excitonic and free carrier components of exciton absorption saturation were analyzed as a function of well width. The relative importance of phase space filling, Coulomb screening and broadening contributions was determined from polarization and laser bandwidth dependencies via spin-dependent and spin-independent components. A five-level model was used to fit the data and nonlinear coefficients for the individual contributions were determined for each well width. The Coulomb contributions arising from screening and broadening of the excitons was found to dominate the absorption bleaching using picosecond pulses, whereas phase space filling was largest in the femtosecond regime. Exciton phase space filling was found to be four times larger than free carrier phase space filling at narrower well widths. A sublinear dependence of exciton broadening with carrier density was observed. © *1999 American Institute of Physics.* [S0021-8979(99)06919-4]

I. INTRODUCTION

Excitons in multiple quantum well (MQW) semiconductors exhibit large resonant optical nonlinearities[1,2] which offer a number of useful functions for optoelectronic devices.[3] These include laser mode-locking elements,[4] saturable elements for controlling the propagation of optical solitons in fiber transmission systems,[5] all-optical bistable etalons,[6] all-optical directional coupler switches,[7] and self-electro-optic devices[8] for high speed communications, signal processing and computing.[9] The operation and optimization of these devices rely on an understanding of the mechanisms that contribute to bleaching of the exciton absorption feature at room temperature. Previous work has shown that the relative contributions of the various mechanisms which cause bleaching can be distinguished by the use of circularly polarized light[10,11] and different laser pulse widths[12] in pump-probe measurements. This article describes pump-probe measurements in GaAs/AlGaAs MQWs using both picosecond and femtosecond duration pulses, as a function of wavelength, polarization, bandwidth, carrier density, and well width in order to quantify the individual contributions to excitonic optical nonlinearities. Three MQW samples with different well widths have been compared in these studies.

II. BACKGROUND

Excitonic absorption features are clearly resolved at room temperature in quantum wells compared to bulk semiconductors because confinement leads to larger binding energies and enhanced oscillator strengths. The loss of degeneracy of light hole (lh) and heavy hole (hh) valence bands leads to an exciton doublet in MQWs. Bleaching of the excitonic features is observed in GaAs/AlGaAs MQWs at below 1 mW average power, for laser spot sizes on the order of 10–100 μm. This saturation occurs due to the optical generation of excitons or free carriers at two-dimensional (2D) densities in excess of $10^{10}\,\mathrm{cm}^{-2}$.

Resonant excitation initially creates bound electron-hole pairs, i.e., excitons. When the density of excitons approaches that required to fill space ($\sim 10^{17}\,\mathrm{cm}^{-3}$ based on an exciton diameter of 30 nm for bulk GaAs), then the number of additional excitons which can be created is reduced by Pauli exclusion, thus decreasing the level of absorption. Knox *et al.*[13] measured a room-temperature ionization time for excitons into free electron-hole pairs of 300 fs. Therefore, on time scales less than 300 fs, bleaching results primarily from the excess exciton density, while on picosecond and longer time scales, it can be assumed that the exciton saturation results from free carriers.

In order to describe the different nonlinearities responsible for exciton saturation, the generalized Wannier equation can be used. This is deduced from the screened Hamiltonian for a two-band, quasi-two-dimensional semiconductor:[11,14,15]

$$[\hbar\omega - E_{e,k} - E_{h,k} + i(\Gamma_0 + \Gamma) + \Sigma_{k,\sigma}]\chi_{k,\sigma} = (1 - f_{e,\sigma,k} - f_{h,\sigma,k})\left[d_k + \sum_{k'} V_s(k-k')\chi_{k',\sigma}\right] \quad (1)$$

for the polarizability $\chi(\hbar\omega) = \Sigma_k d_k \chi_{k,\sigma}(\hbar\omega)$ whose imaginary part is proportional to the absorption coefficient. $E_{e,k}, E_{h,k}$ correspond to the single-particle energies of electron and hole, respectively. $V_s(k)$ is the Fourier transformed quasi-two-dimensional screened Coulomb potential, d_k the dipole moment (proportional to the modulus of the interband momentum matrix element) and $f_{i,\sigma,k}(i=\{e,h\})$ are the Fermi functions describing the distribution of electrons (holes) in their energy bands with spin σ. $\Sigma_{k,\sigma}$, the real part of the self-energy is given by

[a]Electronic mail: a.miller@st-and.ac.uk

$$\Sigma_{k,\sigma}=\sum_{k'}(f_{e,\sigma,k}+f_{h,\sigma,k})V_s(k-k')$$

$$+\sum_{k'}V_s(k')-V(k), \tag{2}$$

where $V(k)$ is the Fourier transformed unscreened potential.

The first term of these summations is the ''exchange hole'' energy and results from the Pauli exclusion principle which implies that each fermion is surrounded by a region where the probability of the existence of another identical fermion is very small. This repulsive energy occurs for particles with equal spin and charge.

The second term is the ''Coulomb hole'' energy which involves equally charged fermions avoiding each other because of Coulomb repulsion. This term is independent of the spin of the particles. A finite homogeneous linewidth Γ_0, is introduced to account for dephasing collisions (electron-phonon interactions) and is accompanied with the term Γ which corresponds to the imaginary part of the self-energy representing the carrier-carrier scattering rate.

Finally, the term $(1-f_{e,\sigma,k}-f_{h,\sigma,k})$ is the filling factor representing a blockade of transitions by Pauli exclusion, where a state occupied by a fermion is no longer available as a final state in an optical absorption process.

We can therefore distinguish three different mechanisms inducing exciton saturation:

Phase space filling (PSF) is the mechanism resulting directly from the Pauli exclusion principle and will reduce the excitonic oscillator strength through the filling factor and the exchange hole energy.

Screening is the mechanism resulting from the Coulomb interaction and will reduce the excitonic oscillator strength through the screened potential V_s and the Coulomb hole energy.

Broadening is the mechanism resulting from carrier-carrier scattering and will increase the homogeneous linewidth of the exciton with the same overall oscillator strength through the imaginary part of the self-energy.

PSF depends on the spin of the electron since the filling factor and the exchange hole energy are both spin-dependent quantities, in contrast to screening and broadening (in the low density regime). This difference has already been exploited in pump-probe experiments in MQWs at room temperature[11,12] where it was possible to separate experimentally the effect of PSF from the combined effects of screening and broadening. This is made possible only in MQW semiconductors because of the lifting of the degeneracy between the light and heavy hole bands due to confinement allowing access to polarization sensitive optical selection rules, as shown in Fig. 1.

Circularly polarized light resonant with the heavy hole exciton generates 100% spin-polarized electron-hole pairs. The initial spin orientation of the optically generated excitons is maintained by the electrons for tens of picoseconds after exciton ionization.[16] Spin relaxation is not a coherent phenomenon. The physics of electron spin relaxation has been analyzed theoretically in bulk[17] and MQW[18] semiconductors at room temperature and is most likely due to the D'Yakonov and Perel (DP) process.[16,17] The DP spin relaxation mechanism results from spin-orbit splitting of the conduction band. Spin splitting is equivalent to the existence of a magnetic field acting on the electron spins. Between collisions the spin precesses about the direction of the pseudofield, defined by the momentum direction. During collisions, changes in momentum cause a rotation of the precession axis, allowing the spins to flip.

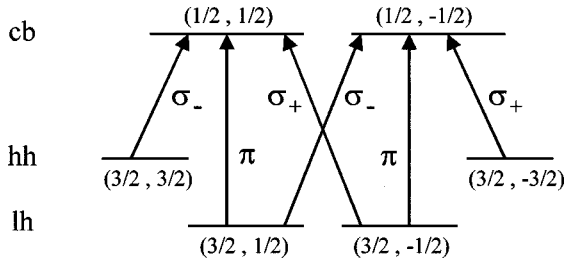

FIG. 1. Selection rules for the transitions from the heavy hole and light hole valence bands to the conduction band in MQWs. The (j, m_j) refer to the quantum numbers for angular momentum and its component along one direction. The σ^+ and σ^- refer to the transitions excited by each sense of circularly polarized light and correspond to $\Delta m_j=\pm 1$, respectively, where the propagation direction is used to define m_j.

Hole spin relaxation is much faster (subpicosecond time scale at room temperature) because of valence band mixing and the mixed spin character of the light hole states.[19,20] Therefore, because PSF is spin dependent, it is possible to separate out electron PSF and to deduce the spin relaxation time for free electrons by studying the change in transmission of the probe as a function of time delay under different polarization combinations of pump and probe. In addition, a study of the change in transmission of the probe as a function of carrier density and excitation wavelength will show the relative importance of broadening as compared to screening. The density dependence of the broadening is complex and not well established theoretically.

III. EXPERIMENT

Pump-probe experiments were carried out using a self-mode-locked Ti:sapphire laser (Spectra-Physics, Tsunami) producing either 100 fs or 1 ps pulses at 82 MHz. The beam was split to form pump and probe pulses, and the time of arrival of the probe pulses at the sample could be varied with a variable optical delay. The pump beam was chopped for subsequent phase sensitive detection. Each of these beams was passed through a linear polarizer followed by a quarter-wave plate or a half-wave plate to produce either left or right handed circularly polarized or linearly polarized light. A set of three samples, S51, KLB, and FK141 were studied.

Sample S51 consists of 60 periods of 4.4 nm GaAs quantum wells surrounded by 17.5 nm $Al_{0.33}Ga_{0.66}As$ barriers with no doping background. KLB contains 120 periods of 6.5 nm GaAs quantum wells surrounded by 21.2 nm $Al_{0.4}Ga_{0.6}As$ barrier with an intentional *p*-type doping background of $\sim 10^{16}\,cm^{-3}$. FK141 incorporates 15 periods of 9 nm GaAs quantum wells surrounded by 10 nm $Al_{0.2}Ga_{0.8}As$ barrier with no doping background.

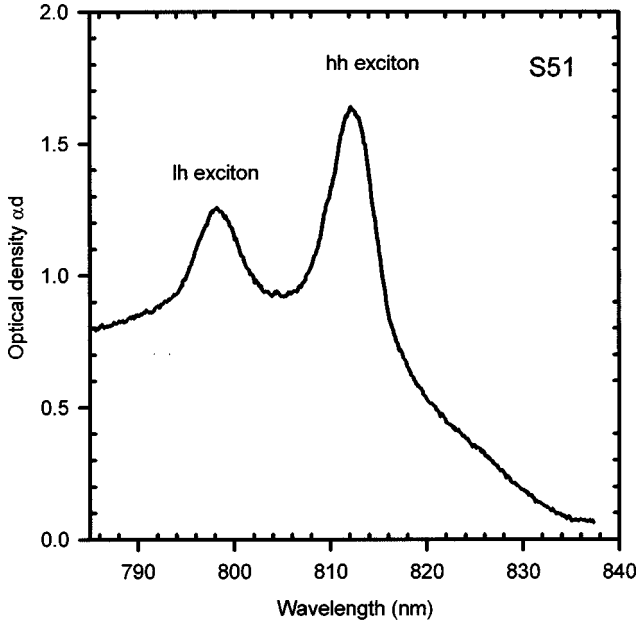

FIG. 2. Optical density, αd, as a function of wavelength for sample S51 at room temperature (hh=heavy hole, lh=light hole)

The GaAs substrate was etched off to allow transmission measurements and an antireflection coating applied to each surface for all three samples. Figure 2 shows the hh-lh exciton doublet in the linear absorption spectrum for sample S51.

A pump power of 1 mW resonant with a hh exciton absorption peak creates an estimated carrier density of $\sim 5 \times 10^{16}\,\mathrm{cm}^{-3}$ for each sample (within a factor 2, taking into account the different absorption coefficients, thicknesses, and well widths). This corresponds to a two-dimensional density of $\sim 10^{10}\,\mathrm{cm}^{-2}$. (Although there will be some nonuniformity of carrier density across the wells, particularly in S51 and KLB, within the low density (linear) regime, this does not affect the results.) We measure the change in transmission ΔT of the probe beam and deduce the change in absorption $\Delta\alpha$ from the relation:

$$\Delta \alpha d = -\ln\left(\frac{\delta T}{T_0}+1\right) \approx -\frac{\Delta T}{T_0}, \tag{3}$$

where d is the effective thickness of the sample and T_0 its linear transmission. For sufficiently small change in transmission, the two quantities are proportional.

IV. WAVELENGTH DEPENDENCE

Bleaching of exciton absorption produces both absorptive and refractive optical nonlinearities at moderate optical powers.[21] There is no observed shift in wavelength of the peak of the exciton during saturation. Any reduction of the binding energy caused by Coulomb screening to yield a blueshift of the exciton is balanced by a redshift resulting from band-gap renormalization.[22] This may not be entirely coincidental, since band-gap renormalization arises from a combination of exchange and correlation effects between carriers which is a Coulomb interaction, plus the fact that the exciton is a neutral particle.[23] Above about 3 mW, the absorption becomes progressively more difficult to saturate because band-gap renormalization causes a redshift of the fundamental band-gap energy and thus a progressively larger density of states needs to be blocked. At high optical powers, and thus very high carrier densities, band filling will cause the remaining absorption to saturate, but this is normally accompanied by a redshift of the band gap due to local heating of the lattice.

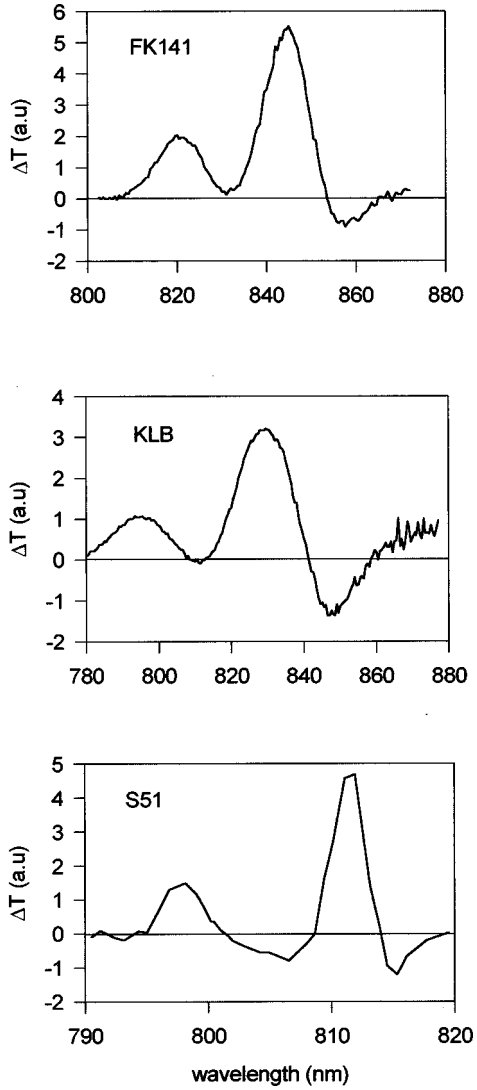

FIG. 3. Change in transmission as a function of the laser wavelength using linear polarization for the three samples FK141, KLB, and S51.

Figure 3 compares differential transmission spectra for the three GaAs/AlGaAs MQW structures with different well widths under conditions of moderate excitation level. These spectra were recorded in a pump-probe configuration using linearly polarized 1 ps duration pulses. There was a fixed delay of a few picoseconds between the pump and probe pulses. The negative signals are caused by broadening of the exciton features. It may be noted that the magnitude of the negative signal is largest in the sample with the narrowest quantum wells and clearly occurs on both sides of the hh exciton feature in this case.

V. POLARIZATION DEPENDENCE

Figure 4 shows the results of time-resolved saturation measurements carried out at the peak of the hh exciton ab-

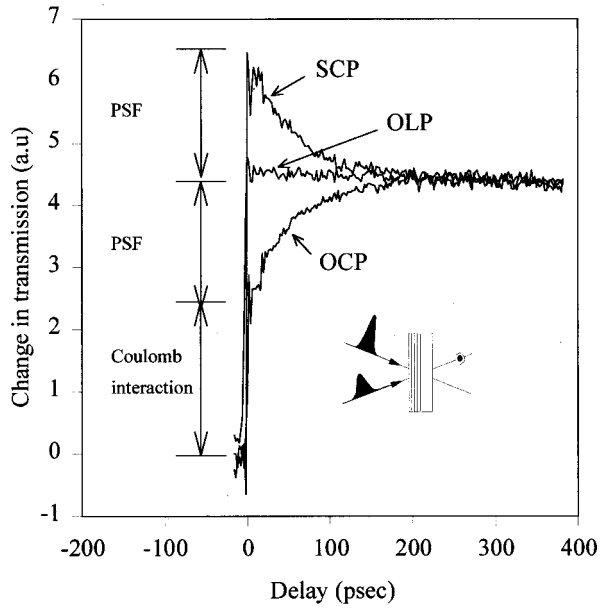

FIG. 4. Dependence of probe transmission change on optical time delay in pump-probe measurements for three polarization configurations, OLP=opposite linear polarization, SCP=same circular polarization, OCP=opposite circular polarization for sample KLB.

sorption in sample KLB at room temperature using 1 ps pulses with the three polarization configurations of pump and probe beams, (a) opposite linear polarization (OLP), (b) same circular polarization (SCP), and (c) opposite circular polarization (OCP). One picosecond pulses have a spectral bandwidth much less than the hh exciton spectral linewidth. The transmission change is due to the combined effects of PSF, screening and broadening on exciton saturation which all reduce the absorption at the center of the line. The OLP configuration shows a rapid rise in transmission of the probe at zero delay followed by a recovery due to carrier recombination on nanosecond time scales. The signal is therefore observed as an almost flat plateau on the picosecond time scales recorded here. (Note that there is no difference using the same and opposite linear polarizations.)

When the pump is circularly polarized, all of the carriers generated will initially have the same spin orientation. The probe can be chosen to have either the same sense of circular polarization as the pump, SCP, or the opposite circular polarization, OCP. The SCP result in Fig. 4 shows an initially enhanced saturation, compared to the OLP case, and a recovery to the plateau level within a time on the order of 100 ps. This enhancement arises from spin-dependent PSF. The probe interacts with electron spin states that are twice as full as those in the OLP case (for the same total number of excited carriers). For the OCP condition, the initial bleaching is less than for OLP. In this case, immediately after excitation all of the electrons are in the opposite spin state to that being probed, so there is no PSF. This results in less bleaching initially, but as the electron spins randomize, the OCP signal rises to the OLP level. The initial level in the OCP signal close to zero delay is due to the combined spin-independent Coulomb effects of screening and broadening. The recovery time of the enhanced (SCP) and reduced (OCP) bleaching gives a characteristic electron spin relaxation time τ_{spin} of 50 ps.

For the OCP configuration, the combined influence of PFS, screening, and broadening sets the transmission change at the plateau level, whereas the initial change in transmission before any spin relaxation occurs, is due to screening and broadening alone. Again for the SCP configuration, the difference between the plateau level and the initial signal is solely due to PSF. We note that the influence of PSF in the SCP configuration, is roughly double that in the OLP configuration. This is because there is only one electron available per state (all of the electrons have the same spin in the SCP configuration) compared to the OLP configuration in which both spin states are excited. As a result, for the same generated electron population, there will be twice as many occupied states in the probed spin band in the SCP case as compared to the OLP case, doubling the influence of PSF. Although the general equation [Eq. (1)] relates the different mechanisms in a complex manner, calculations have been performed,[11] that well describe the results obtained for the three different polarization configurations in pump-probe measurements in a low density regime ($<10^{10}\,\text{cm}^{-2}$).

We have been able to separate PSF due to electrons in this experiment only because the hole spin randomizes within 1 ps at room temperature. It is possible that PSF due to the holes occurs even in the OCP configuration. However, the average in-plane effective mass for holes is much larger than for electrons, which means that PSF should be dominated by the electron contribution. Furthermore, calculations show only a small difference when PSF induced by the holes is taken into account.

VI. SPECTRAL BANDWIDTH DEPENDENCE

The broad bandwidth of ultrashort pulses can be used to identify the broadening contribution to the exciton absorption nonlinearity as described by Holden *et al.*[12] Figures 5(a) and 5(b) compare results of pump-probe measurements (as described in Sec. V) using 1 ps and 100 fs pulses for sample S51. One picosecond pulses have a spectral bandwidth of $\sim$ 2 meV, so that the observed transmission change centered on the peak of the hh exciton of spectral linewidth 6.4 meV (see Fig 2), is due to the combined effects of PSF, screening and broadening. On the other hand, for 100 fs pulses, the measured bandwidth is $\sim$ 10 nm (20 meV), which is greater than the hh exciton absorption linewidth. Consequently, 100 fs duration probe pulses effectively measure the integrated absorption change rather than the change at the line center. The striking difference between the two sets of results in Figs. 5(a) and 5(b) follows from the absence of any sensitivity to broadening of the exciton when using the shorter duration pulses. Collisional broadening lowers the absorption at line center while it increases it in the wings leaving the integrated absorption unchanged. A comparison of the initial step sizes for the OCP configuration for picosecond results, Fig. 5(a), and femtosecond results, Fig. 5(b), demonstrates that broadening is the dominant contribution to the peak exciton absorption quenching in this sample for picosecond or longer duration pulses.

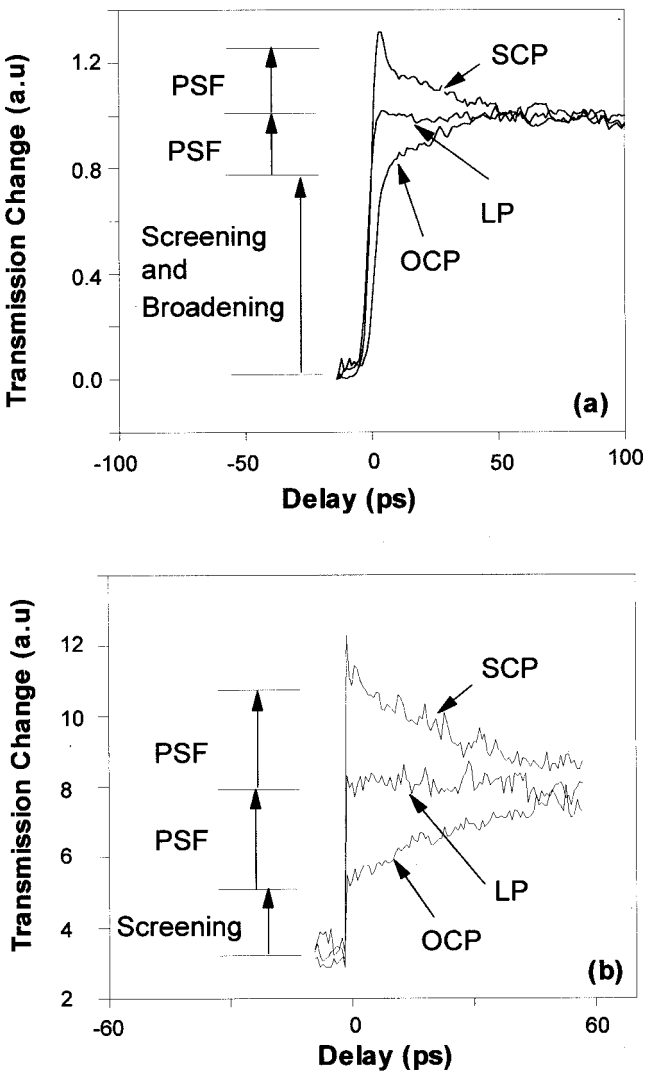

FIG. 5. Probe transmission changes as a function of delay time for the three polarizations, SCP, LP, and OCP using (a) 1 ps and (b) 100 fs pulses for sample S51.

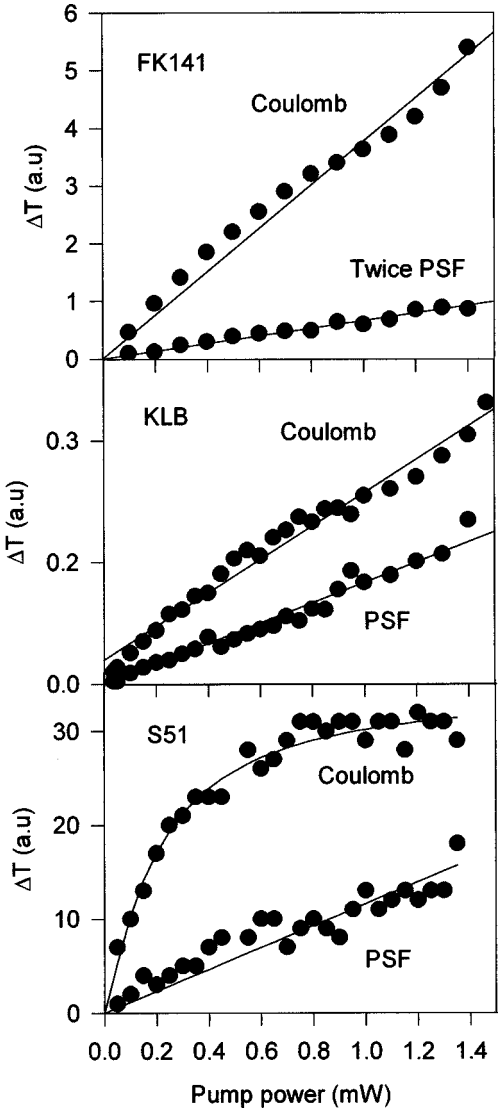

FIG. 6. Coulomb (screening and/or broadening) and PFS contributions to the transmission changes as a function of the pump power at the peak of the heavy hole exciton in the three samples FK141, KLB, and S51.

VII. CARRIER DENSITY DEPENDENCE

So far, we have identified broadening to be the most significant contribution to exciton bleaching in the sample with the narrowest wells (S51) using longer duration pulses from the wavelength dependence and from the laser bandwidth dependence in polarization sensitive pump-probe studies. Broadening can also be identified in measurements carried out as a function of pump power when the polarization selection rules are again used to extract the magnitude of the spin-independent contribution to exciton saturation.

Results such as those shown in Fig. 4 using 1 ps pulses were used to quantify the relative magnitudes of the electron PSF and Coulomb contributions to exciton saturation at low excitation from the initial changes in transmission in the three polarization configurations. We now extend this to study the variation as a function of generated excess carrier density. Figure 6 plots the spin-dependent (PSF) and spin-independent (Coulomb) components of the initial transmission change of 1 ps pulses as a function of the average pump power from results similar to those shown in Fig. 4 for the three MQW samples.

First, we note that the Coulomb contribution is always larger than the PSF contribution for all three well widths. Second, the power dependence is observed to be linear in all cases except for the Coulomb contribution in sample S51.

In all three samples, the spin-independent component, ΔT_{PSF}, increases linearly with the carrier density. This implies that the excitonic oscillator strength decreases linearly with carrier density (up to $10^{10}\,\mathrm{cm}^{-2}$) as expected for a third-order nonlinearity. The experiment remains in a low density regime because the excitonic absorption is not completely saturated.

For samples KLB and FK141, the spin-independent component, ΔT_{OCP}, follows the same linear dependence as PSF. This similar behavior is expected for the screening mechanism and has been calculated previously.[12] This component is significantly larger than PSF and is found to be more dominant in FK141 than in KLB in comparison with

PSF. One possible explanation would be the influence of confinement. In fact, the quantum wells in sample KLB have a well width of 6.5 nm with an electron confinement energy of 63 meV, whereas the wells in FK141 are 9 nm wide with an electron confinement energy of 37 meV. Previous theoretical studies[12] predicted that PSF should increase its influence with confinement and become the dominant mechanism. This evolution is consistent with our measurements, with the exception that the spin-independent component remains larger than PSF although its influence decreases with confinement.

The carrier density dependence of the spin-independent Coulomb contribution is strongly sublinear in the narrow quantum well sample, S51. We propose that the dominant contribution is broadening whereas screening dominates in the other two samples. This is supported by the negative changes in transmission as a function of wavelength as shown in Fig. 2 in which the broadening mechanism clearly appears in sample S51 at the hh exciton but is not as important in KLB or FK141. This observation indicates that for samples KLB and FK141 the two principal mechanisms for saturation using picosecond pulses are screening and PSF, whereas broadening plays a more important role for S51.

For sample S51, ΔT_{OCP} shows a clear nonlinear behavior. The change in transmission varies linearly up to a pump power of $\sim$ 0.2 mW which corresponds to a carrier density of $\sim 3\times 10^{9}\,\mathrm{cm}^{-2}$ and is followed by a saturation effect. If we assume an exciton resonance centered at the wavelength $\lambda_{\max}$ to have a Gaussian shape, the absorption will be

$$\alpha d = \alpha_0 d \exp\left(- \frac{(\lambda - \lambda_{\max})^2}{\Gamma'^2} \right), \tag{4}$$

where Γ' is the linewidth of the resonance. If we consider broadening to be the only mechanism, we have the relation at $\lambda = \lambda_{\max}$:

$$\Gamma' = \frac{\Gamma_0 \alpha_0 d}{\alpha_0 d - \ln(\Delta T / T_0 + 1)}, \tag{5}$$

where Γ_0 and α_0 are the initial linewidth and absorption coefficient before the pump excitation. For relatively small changes in transmission and with a coefficient $\alpha_0 d$ close to unity, relation Eq. (5) becomes

$$\frac{\Gamma}{\Gamma_0} = \frac{\Gamma' - \Gamma_0}{\Gamma_0} \approx \frac{\Delta T}{\alpha_0 d T_0}. \tag{6}$$

As a result, ΔT_{OCP} gives a measure of the change of the exciton linewidth. Γ corresponds to the same collision rate as defined in Eq. (1). In general, scattering of the exciton is caused by exciton-exciton and exciton-free carrier interactions. A direct measurement of collisional broadening of excitons in GaAs quantum wells has been reported at low temperatures,[24] showing separately the scattering induced by free carriers and excitons. The free carrier-exciton scattering rate has been observed to increase linearly up to a carrier density of $5\times 10^{9}\,\mathrm{cm}^{-2}$ as predicted by many-body theory at low density.[25] At room temperature, excitons ionize within 300 fs which implies that the dominant scattering mechanism contributing to the increased exciton linewidth will be exciton-free carrier collisions. Our measurements are consistent with the low temperature measurements of Ref. 24, but as the carrier density increases above $\sim 5\times 10^{9}\,\mathrm{cm}^{-2}$, the collision rate begins to saturate. Many-body theory is not well established for a correct description of the scattering rates and phenomenological dependencies are usually introduced if this effect has to be taken into account.[11] We can, however, understand this behavior qualitatively. As the density of carriers becomes more significant, the number of scattering events per unit volume increases in proportion to the carrier density; but simultaneously the carrier-carrier interaction, which is nothing but the Coulomb interaction, is screened, thereby reducing the impact of any collision above a critical density. From this point of view, the screening mechanism, as it has been defined in this paper, and the broadening mechanism have the same physical origin, i.e., the Coulomb interaction. Screening corresponds to the effect of Coulomb interaction on the oscillator strength, whereas broadening corresponds to the effect of Coulomb interaction on the resonance linewidth.

In this analysis for sample S51, we have assumed that the only mechanism that contributes to ΔT_{OCP} is broadening. However, the screening mechanism should also be included as indicated by the spectral bandwidth results discussed in Sec. VI. From Fig. 5(b), the contribution due to screening is about two thirds of the PSF contribution, so that the broadening can be estimated from Fig. 5(a) at around five times that of screening at low excitation levels. The quantum wells in sample S51 are 4.4 nm wide, with an electron confinement energy of 93 meV. From the analysis of KLB and FK141, we expect the screening mechanism to be linearly dependent on carrier density and to have a maximum value of the same order of magnitude as PSF. However, such a correction due to screening would have the effect of reinforcing the saturation characteristic of the curve. Besides, we have measured in single beam experiments that the maximum change in transmission for S51 reaches 15% compared with only 5% for KLB, indicating that the effect of screening on ΔT is not as strong as the effect of broadening in S51.

As illustrated in Fig. 2, S51 is of high optical quality with a sharp well-resolved heavy hole exciton at room temperature ($\Gamma_0 = 6.4\,\mathrm{meV}$). This is partly due to good material quality and partly because the well width of 4.4 nm gives close to the maximum exciton binding energy. Therefore, a small change of the linewidth can induce a rather large change in transmission at the maximum of the resonance. On the other hand, the excitonic absorption features in KLB and FK141 are not as well resolved which make the broadening mechanism less sensitive for these two samples. Moreover, the broadening effect may become more important with more confinement but there is no theory available for such a prediction.

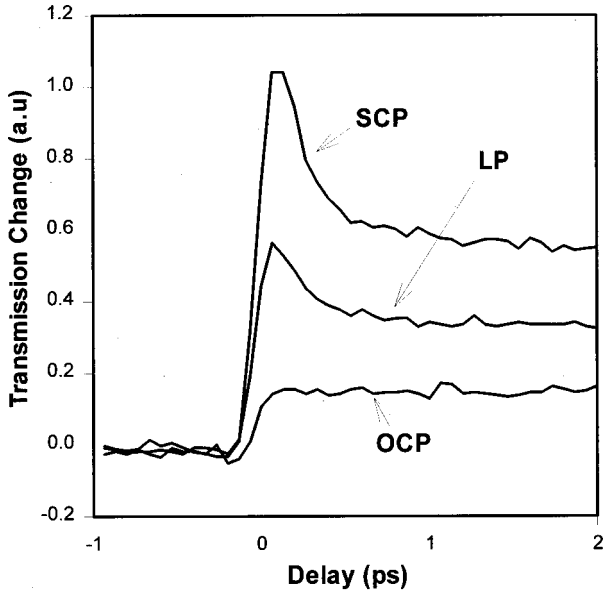

FIG. 7. Probe transmission changes at the hh exciton absorption peak as a function of delay using 100 fs pulses for SCP (same circular polarizations), LP (same linear polarizations), and OCP (opposite circular polarizations) as a function of time for sample S51.

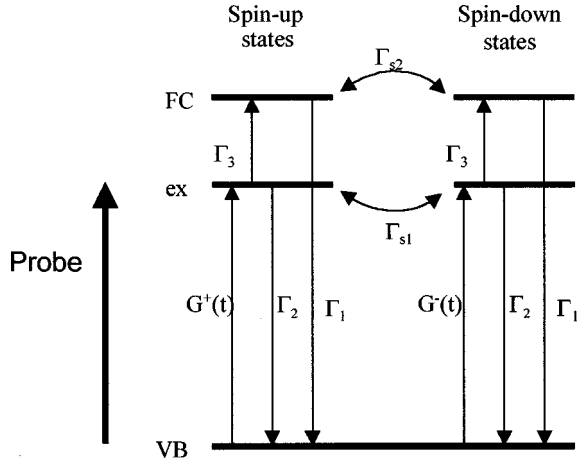

FIG. 8. Diagram of the five-level system. The arrows represent the direction of flow of population.

VIII. TIME DEPENDENCE

Higher time resolution pump-probe measurements using 100 fs pulses allow a comparison of exciton absorption saturation before and after exciton ionization.[12,13] In this section, we will describe an analysis of pump-probe results, which gives the relative magnitudes of exciton and free carrier contributions to spin-dependent and spin-independent hh exciton bleaching. Using 100 fs pulses, broadening is averaged out and the contributions from free carrier phase space filling (spin dependent) and free carrier Coloumb screening (spin independent) can be isolated and compared. Circular polarizations were again employed in order to create and probe these spin-dependent and spin-independent mechanisms.

An example of a set of higher time resolution pump-probe scans using 100 fs pulses and recorded within 2 ps of zero delay are shown in Fig. 7. In his case, a probe beam steering mirror was vibrated to eliminate any coherence artifacts. Resonant excitation with a 100 fs pulse initially produces a population of cold ($k=0$) bound electron-hole pairs (excitons). Further creation of excitons is inhibited by excitonic PSF and thus the absorption becomes bleached. At room temperature, excitons strongly ionize via collisions with LO phonons within about 300 fs.[13] A fast transient feature is seen in SCP and LP configurations in Fig. 7, as the excitons are rapidly generated and then ionize, creating hot free carriers. Within the first 1 ps after excitation, exciton contributions have passed and free carrier contributions to exciton saturation dominate. The enhanced transmission change at small delays results from the fact that the presence of excitons is more efficient in saturating the hh exciton absorption feature than the presence of the same density of free carriers. This transmission enhancement is observed to be larger for the SCP configuration than LP, confirming that the spin-dependent PSF component is larger for excitons than for free carriers.

On inspection of the OCP trace in Fig. 7, the initial rise shows a step followed by a slow increase in transmission towards the LP curve at the spin reorientation rate. Perhaps surprisingly, there is no signature of exciton ionization. As PSF does not contribute to the initial OCP condition, this observation may indicate that screening due to excitons and free carriers is equal.[12] However, an alternative interpretation is that the exciton contribution is minimal because the correlated opposite charge carriers cancel each other out.[26] In this latter case, the initial rise in the OCP transmission is due only to the free carrier population build up after exciton ionization. The theoretical fits for the OCP data described later are highly sensitive to the pulse duration and the zero delay position. Further experiments are needed to determine the precise relative magnitude of the exciton screening.

The schematic in Fig. 8 shows a five-level model containing two coupled three-level systems, one for spin-up and one for spin-down carriers with a common ground state. The coefficients Γ_1 and Γ_2 correspond to the recombination rates of the free carriers and excitons and Γ_3 gives the rate of exciton ionization. The inverses of these coefficients give the characteristic ionization or relaxation times. Another factor changing the carrier populations is the pump excitation. This excitation is represented by intensity profiles of the pulse decomposed into the two opposite circular polarization $G^+(t)$ and $G^-(t)$. The selection rules, Fig. 1, imply that $G^+(t)$ and $G^-(t)$ correspond to the rate of excitation of the carriers from the ground level into the spin-up and spin-down exciton levels, respectively. Further, we take into account the spin relaxation rates Γ_{s1} and Γ_{s2}, which imply a homogenization of the spin after the selective excitation of only one spin state. Finally, the probe pulse is represented here to be resonant with the spin-up exciton level.

The evolution of the population of such a five-level system is given by a system of four coupled first-order differential equations

$$\begin{aligned}
\frac{dn_{\mathrm{ex}}^{+}}{dt} &= -(\Gamma_2+\Gamma_3+\Gamma_{s1})n_{\mathrm{ex}}^{+}+\Gamma_{s1}n_{\mathrm{ex}}^{-}+G^{+}(t),\\
\frac{dn_{\mathrm{ex}}^{-}}{dt} &= +\Gamma_{s1}n_{\mathrm{ex}}^{+}-(\Gamma_2+\Gamma_3+\Gamma_{s1})n_{\mathrm{ex}}^{-}+G^{-}(t),\\
\frac{dn_{\mathrm{FC}}^{+}}{dt} &= +\Gamma_3 n_{\mathrm{ex}}^{+}-(\Gamma_1+\Gamma_{s2})n_{\mathrm{FC}}^{+}+\Gamma_{s1}n_{\mathrm{FC}}^{-},\\
\frac{dn_{\mathrm{FC}}^{-}}{dt} &= +\Gamma_3 n_{\mathrm{ex}}^{-}+\Gamma_{s2}n_{\mathrm{FC}}^{+}-(\Gamma_1+\Gamma_{s2})n_{\mathrm{FC}}^{-},
\end{aligned} \tag{7}$$

where n_{ex}^{+}, n_{ex}^{-}, n_{FC}^{+}, and n_{FC}^{-} represent the exciton and free carrier populations in the spin-up and spin-down states.

In order to find a simple analytic solution to this system of equations, we assume that the intensity profile of the excitation is Gaussian. We can distinguish three different modes of excitation, which can be summarized into the following expressions:

$$\begin{aligned}
G^{+}(t) &= g_0^{+}\exp\left(-\frac{t^2}{\Delta t_0^2}\right),\\
G^{-}(t) &= g_0^{-}\exp\left(-\frac{t^2}{\Delta t_0^2}\right),
\end{aligned} \tag{8}$$

where $g_0^{\pm}$ and Δt_0 corresponds, respectively, to the intensity coefficient and duration of the pump pulses. In the case of linear polarized light, we have

$$g_0^{-}=g_0^{+}=1/2. \tag{9}$$

For circular polarized light, either the spin-up or spin-down exciton level is excited. For the spin-up excitation, we have

$$g_0^{+}=1, \quad g_0^{-}=0, \tag{10}$$

and for the spin-down case,

$$g_0^{+}=0, \quad g_0^{-}=1. \tag{11}$$

To solve Eq. (7) we transform it into two uncoupled systems each corresponding to a three-level system. Introducing the sum and difference of populations

$$\begin{aligned}
\sigma_{\mathrm{ex}} &= n_{\mathrm{ex}}^{+}+n_{\mathrm{ex}}^{-}, \quad \sigma_{\mathrm{FC}}=n_{\mathrm{FC}}^{+}+n_{\mathrm{FC}}^{-},\\
\delta_{\mathrm{ex}} &= n_{\mathrm{ex}}^{+}-n_{\mathrm{ex}}^{-}, \quad \delta_{\mathrm{FC}}=n_{\mathrm{FC}}^{+}-n_{\mathrm{FC}}^{-},
\end{aligned} \tag{12}$$

the evolution equations of the two three-level systems read

$$\begin{aligned}
\frac{d}{dt}\sigma_{\mathrm{ex}} &= -(\Gamma_2+\Gamma_3)\sigma_{\mathrm{ex}}+G^{+}(t)+G^{-}(t),\\
\frac{d}{dt}\sigma_{\mathrm{FC}} &= +\Gamma_3\sigma_{\mathrm{ex}}-\Gamma_1\sigma_{\mathrm{FC}},
\end{aligned} \tag{13}$$

and

$$\begin{aligned}
\frac{d}{dt}\delta_{\mathrm{ex}} &= -(\Gamma_2+\Gamma_3+2\Gamma_{s1})\delta_{\mathrm{ex}}+G^{+}(t)-G^{-}(t),\\
\frac{d}{dt}\delta_{\mathrm{FC}} &= +\Gamma_3\delta_{\mathrm{ex}}-(\Gamma_1+2\Gamma_{s2})\delta_{\mathrm{FC}}.
\end{aligned} \tag{14}$$

By analyzing these two systems of equations, we see that they correspond indeed to simple three-level systems.

In the σ system, Eq. (13), the excitation is given by the sum of $G^{+}(t)$ and $G^{-}(t)$ and is further characterized by exciton recombination and ionization rates, Γ_2 and Γ_3. The free carrier recombination rate is Γ_1. We remark that all three excitation configurations [Eqs. (9)–(11)] have the same effect on the σ system and thus this system is invariant with respect to the polarization. Indeed, this is to be expected because of the symmetry of switching between spin-up and spin-down states.

Similarly, in the δ system, Eq. (14), the exciton term, δ_{ex}, has recombination and ionization rates given by $(\Gamma_2+2\Gamma_{s1})$ and Γ_3. The ''free carrier'' recombination rate is $(\Gamma_1+2\Gamma_{s2})$. Its excitation corresponds to the difference between $G^{+}(t)$ and $G^{-}(t)$. In this case, the system is not excited at all by the linear polarization excitation, Eq. (9), whereas the circular polarization excitation corresponds either to a ''positive,'' Eq. (10), or ''negative,'' Eq. (11), excitation.

To determine the solution of Eqs. (13) and (14), we need to assume the initial conditions, i.e., the state of the populations before the excitation pulse. We take them to be zero at $t=-\infty$. The exact solutions read

$$\begin{aligned}
\sigma_{\mathrm{ex}}(t) &= (g_0^{+}+g_0^{-})K_{\Gamma_2+\Gamma_3}(t),\\
\sigma_{\mathrm{FC}}(t) &= (g_0^{+}+g_0^{-})[K_{\Gamma_1}(t)-K_{\Gamma_2+\Gamma_3}(t)],\\
\delta_{\mathrm{ex}} &= (g_0^{+}-g_0^{-})K_{\Gamma_2+\Gamma_3+2\Gamma_{s1}}(t),\\
\delta_{\mathrm{FC}} &= (g_0^{+}-g_0^{-})[K_{\Gamma_1+2\Gamma_{s2}}(t)-K_{\Gamma_2+\Gamma_3+2\Gamma_{s1}}(t)],
\end{aligned} \tag{15}$$

where

$$\begin{aligned}
K_{\Gamma}(t) = \frac{\sqrt{\pi}}{2}\Delta t_0 \exp&\left(-\Gamma t+\frac{\Gamma^2\Delta t_0^2}{4}\right)\\
&\times\left[1+\mathrm{erf}\left(\frac{2t-\Gamma\Delta t_0^2}{2\Delta t_0}\right)\right].
\end{aligned} \tag{16}$$

Using the population evolution of Eqs. (15) and (12), we can define the induced transmission change of the probe beam due to the saturation effects. Indeed the density of excitons, and subsequently free carrier pairs, created by the pump pulse under the conditions described in earlier sections was estimated to be $10^{10}\,\mathrm{cm}^{-2}$. At this density, Boltzmann statistics apply and we can assume that the strength of the saturation and transmission change is proportional to the instantaneous particle density. Thus, using the variable delay τ between the pump and probe pulses, one can scan the population evolution after an excitation. The transmission change of the probe pulse is given by the integration of the saturation effects over the duration of the pulse and is proportional to

$$\begin{aligned}
\Delta T(\tau) \propto \int_{-\infty}^{+\infty} G^{+}(t-\tau)[&p_{\mathrm{ex}}n_{\mathrm{ex}}^{+}(t)+(s_{\mathrm{FC}}+p_{\mathrm{FC}})n_{\mathrm{FC}}^{+}(t)\\
&+s_{\mathrm{FC}}n_{\mathrm{FC}}^{-}(t)]dt,
\end{aligned} \tag{17}$$

where the coefficients in front of the populations give the amount of interaction with the probe pulse. Further, in the case of free carriers, we take two contributions into account.

One is due to the screening effect, s_{FC}, and is present for both spin-up and spin-down populations of free carriers. The other part corresponds to the magnitude of the PSF, p_{FC}, and thus is only present on the spin-up side if the circularly polarized probe pulses are probing this transition. In the case of exciton populations, we include only a PSF contribution, p_{ex}, because the screening effects are negligible.

Another benefit of using Gaussian intensity profiles for the excitation pulse is that it is possible to evaluate the integral given by Eq. (17) exactly. To simplify the solution we considered the recombination rates Γ_1 and Γ_2 and the spin relaxation rates Γ_{s1} and Γ_{s2} to be negligible in comparison with the ionization rate Γ_3. This has no effect on the calculated transmission change because of the large difference between these rates.

After simplification, the transmission change is proportional to

$$\Delta T(\tau) \propto p_{ex} g_0^+ K^l_{\Gamma_3}(\tau) + s_{FC}(g_0^+ + g_0^-)[K^l_{\Gamma_1}(\tau) - K^l_{\Gamma_3}(\tau)] + p_{FC}[\tfrac{1}{2}(g_0^+ + g_0^-)K^l_{\Gamma_1}(\tau) - g_0^+ K^l_{\Gamma_3}(\tau) + (g_0^+ - g_0^-)K^l_{2\Gamma_{s2}}(\tau)] \quad (18)$$

with

$$K^l_\Gamma(\tau) = \exp(-\Gamma\tau)\left[1 + \mathrm{erf}\left(\frac{\tau - \Gamma\Delta t_0^2}{\sqrt{2}\Delta t_0}\right)\right]. \quad (19)$$

Both short scan pump-probe measurements with a probe delay of a few picoseconds, Fig. 9, and long scans of up to 120 ps, Fig. 10, were carried out for the three samples using 100 fs pulses. In this way, both the exciton ionization transient and spin relaxation were time resolved. The experimental data from scans on both time scales were then fitted simultaneously using the three pump configurations for each. This greatly improved the parameter confidence, as the spin relaxation times derived from the opposite and same circular polarization must be the same for each sample. Further, the simultaneous fit of the three polarization configurations made possible the determination of the relative contributions of screening and PSF to exciton saturation. In Fig. 9, which shows the short time scale scans for sample S51, we have plotted the individual contributions from spin-up and spin-down excitons and free carriers, as well as the resulting totals. Figure 9(a) and 9(b) show that it takes almost 1 ps for the free carrier concentration to become established. For times less than 1 ps, both exciton and free carrier densities must be taken into account. An exciton ionization time of around 250 fs was determined from the decays in the initial peaks for SCP and LP results. The decays in the longer time scale results in Fig. 10 are determined by spin relaxation, and clearly show the well width dependence of the spin reorientation time by a comparison of the three samples.

We summarize the results of the fits for the three samples using 100 fs pulses in Table I. The magnitudes of the contributions have been normalized to the free carrier screening component in order to illustrate trends in the saturation components as a function of well width. We stress that it is important to carry out this fitting procedure rather than

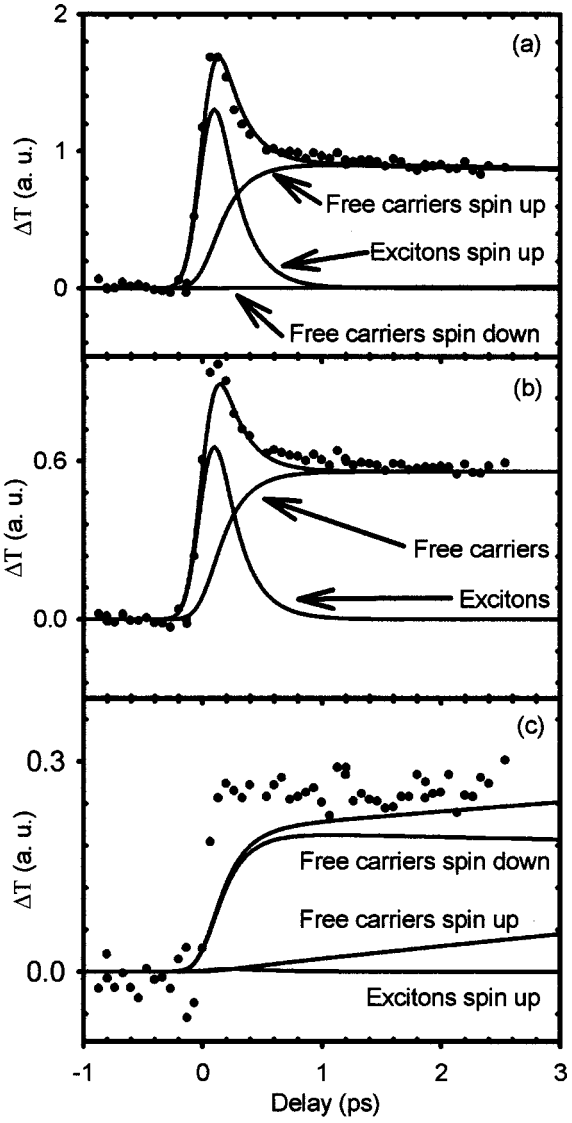

FIG. 9. Change of probe transmission as a function of delay time using 100 fs pulses for sample S51 using the same three polarization configurations as Fig. 7(a) SCP, (b) LP, and (c) OCP. The solid lines are fits to the experimental data (dots). Also shown are the components of the contributions to the transmission change from spin-up and spin-down free carriers and excitons deduced from the fits assuming the probe is coupled to the spin-up states (Fig. 8).

estimate the step sizes in the pump-probe data, in order to accurately determine the relative importance of the different components. Note that the parameters, s_{FC}, p_{FC}, and p_{ex} were defined above [Eq. (17)] as nonlinear coefficients per excess electron-hole pair. This definition gives values of p_{FC} and p_{ex} which are twice as large as the nonlinear coefficients defined with respect to the polarization dependence in Fig. 4 (see Holden *et al.*[12]).

We first note that both the exciton and free carrier PSF contributions are always larger than the spin-independent free carrier Coulomb contribution. This is contrary to the results shown in Fig. 6 obtained with picosecond pulses. In this case, broadening has been eliminated using 100 fs pulses. These results therefore imply that broadening must provide some contribution to the Coulomb component for FK141 and KLB in Figs. 6(a) and 6(b), but the linear density

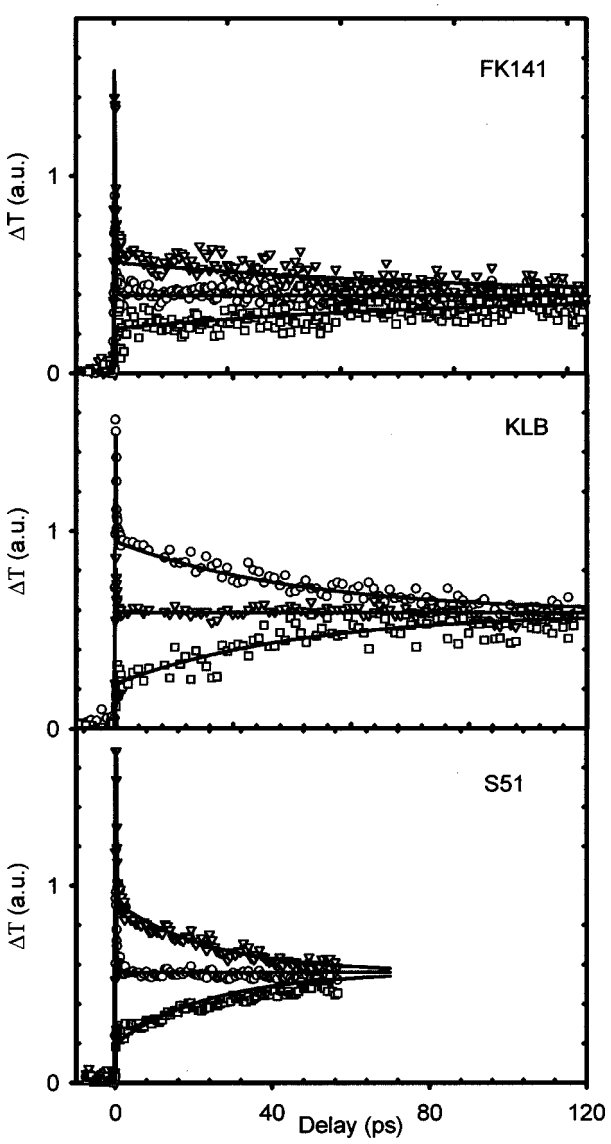

FIG. 10. Change of probe transmission using 100 fs pulses at long time delays for samples FK141, KLB, and S51 together with numerical fits (solid lines) for the three polarization configurations as defined in Fig. 7.

dependencies point to the dominance of the screening component. From Table I, it can be observed that when broadening is eliminated, the ratio of free carrier PSF to screening is greater than unity for all three samples, ranging from 1.5 to 3.6 as the confinement increases.

TABLE I. Results of fitting pump-probe data using 100 fs pulses. p_{FC} and p_{ex} are the relative magnitudes of the PSF contributions to exciton bleaching per electron-hole pair due to free carriers and excitons, respectively, normalized to the free carrier screening contribution per electron-hole pair, s_{FC}. τ_{spin} is the fitted spin relaxation.

Sample	Well width (nm)	s_{FC}	p_{FC}	p_{ex}	p_{ex}/p_{FC}	τ_{spin} (ps)
FK141	9.0	1 ± 0.05	1.5 ± 0.1	11.1 ± 0.5	7.4	180 ± 15
KLB	6.5	1 ± 0.05	3.2 ± 0.1	13.2 ± 0.3	4.1	90 ± 10
S51	4.4	1 ± 0.03	3.6 ± 0.1	14.0 ± 0.2	3.9	50 ± 5

Second, the results in Table I show that, consistent with theory,[26] both p_{FC} and p_{ex} increase with confinement. Exciton PSF is larger than free carrier PSF (for equal excitation densities) for all three well widths, but the ratio of these contributions decreases with increasing confinement. A possible explanation may be found by referring again to Eq. (1). We stated in Sec. II that PSF comprises both a filling factor and an exchange term. We may expect the free carrier contribution to be primarily via the filling factor whereas both terms will contribute in the presence of excess excitons. This follows from the fact that cold excitons will have a higher repulsive potential because they are more highly localization than free carriers. Additionally, whereas optically generated excitons are created close to $k=0$, the free carriers created by thermal ionization of excitons will occupy a range of k states thus reducing the filling factor. Greater quantum confinement will serve to increase the localization of the free carriers thus making the exchange part relatively more important.

Finally, we observe that the well width dependence of the spin relaxation time is consistent with the DP model as reported by Britton *et al.*[16]

IX. CONCLUSION

In these studies, the three main mechanisms responsible for the heavy hole exciton saturation in MQWs at room temperature, i.e., PSF, screening, and broadening, have been studied in samples with different well widths using the pump-probe technique. Both picosecond and femtosecond pulses were employed in experiments carried out as a function of wavelength, polarization, and excitation level. We have shown that the broadening mechanism plays a dominant role for picosecond and longer pulses when the hh exciton absorption resonance is narrow, and we have demonstrated for the first time a saturation of the carrier-carrier collision rate at low density ($\sim 5\times10^{9}\,\mathrm{cm}^{-2}$). This is of importance for any optoelectronic device using room temperature excitonic nonlinearities in quantum wells. In addition, measurements such as four-wave mixing which involve resonant excitonic optical nonlinearities must be interpreted appropriately in the light of this observation. In samples where broadening is less important, we have shown that screening remains an important contribution although PSF becomes increasingly dominant in narrower wells. Excitonic PSF is approximately four times larger than the free carrier component in narrower wells.

ACKNOWLEDGMENTS

The authors would like to thank Ian Galbraith for useful discussions and Karl Woodbridge, Geoff Duggan, and Don McDaniels for the MQW samples used in these studies. EPSRC is acknowledged for financial support.

[1] *Optical Nonlinearities and Instabilities in Semiconductors,* edited by H. Haug (Academic, San Diego, 1988).
[2] S. Schmitt-Rink, D. S. Chemla, and D. A. B. Miller, Adv. Phys. **38**, 89 (1989).

[3] A. Miller, in *Fabrication, Properties and Applications of Low-dimensional Semiconductors*, edited by M. Balkanski and I. Yanchev (Kluwer, Dordrecht, 1995), pp. 383–413.
[4] U. Keller, W. H. Knox, and G. W. 'tHooft, IEEE J. Quantum Electron. **28**, 2123 (1992).
[5] D. Atkinson, W. H. Loh, V. V. Afansjev, A. B. Grudinin, S. J. Seeds, and D. N. Payne, Opt. Lett. **19**, 1514 (1994).
[6] T. Rivera, F. R. Ladan, A. Izrael, R. Azoulay, R. Kuszelewicz, and J.-L. Oudar, Appl. Phys. Lett. **64**, 869 (1994).
[7] S. Shi, P. LiKamWa, A. Miller, J. Pamulapati, P. Cooke, and M. Dutta, Appl. Phys. Lett. **66**, 79 (1995).
[8] D. A. B. Miller, Opt. Quantum Electron. **22**, S61 (1990).
[9] A. L. Lentine, L. M. F. Chirovsky, L. A. D'Asaro, C. W. Tu, and D. A. B. Miller, IEEE Photonics Technol. Lett. **1**, 129 (1989).
[10] A. Takeuchi, S. Muto, T. Inata, and T. Fujii, Appl. Phys. Lett. **56**, 2213 (1990).
[11] M. J. Snelling, P. Perozzo, D. C. Hutchings, I. Galbraith, and A. Miller, Phys. Rev. B **49**, 17160 (1994).
[12] T. M. Holden, G. T. Kennedy, A. R. Cameron, P. Riblet, and A. Miller, Appl. Phys. Lett. **71**, 936 (1997).
[13] W. H. Knox, R. L. Fork, M. C. Downer, D. A. B. Miller, D. S. Chemla, C. V. Shank, A. C. Gossard, and W. Weigmann, Phys. Rev. Lett. **54**, 1306 (1985).
[14] H. Haug and S. W. Koch, *Quantum Theory of the Optical and Electronic Properties of Semiconductors* (World Scientific, London, 1993).
[15] M. Lindberg and S. W. Koch, Phys. Rev. B **38**, 3342 (1988).
[16] R. S. Britton, T. Grevatt, A. Malinowski, R. T. Harley, P. Perozzo, A. R. Cameron, and A. Miller, Appl. Phys. Lett. **73**, 2140 (1998).
[17] M. I. D'Yakonov and V. I. Perel, Zh. Eksp. Teor. Fiz. **60**, 1954 (1971) [Sov. Phys. JETP **33**, 1053 (1971)].
[18] M. I. D'Yakonov and V. Yu. Kachorovskii, Sov. Phys. Semicond. **20**, 110 (1986).
[19] R. Ferreira and G. Bastard, Phys. Rev. B **43**, 9687 (1991).
[20] A. Tkeuchi, Y. Nishikawa, and O. Wada, Appl. Phys. Lett. **68**, 797 (1996).
[21] A. Miller, R. J. Manning, P. K. Milsom, D. C. Hutchings, D. W. Crust, and K. Woodbridge, J. Opt. Soc. Am. B **6**, 567 (1989).
[22] C. Weber, C. Klingshirn, D. S. Chemla, D. A. B. Miller, J. E. Cunningham, and C. Ell, Phys. Rev. B **38**, 12748 (1988).
[23] S. Schmitt-Rink, D. S. Chemla, and D. A. B. Miller, Adv. Phys. **38**, 89 (1989).
[24] A. Honold, L. Schultheis, J. Kuhl, and C. W. Tu, Phys. Rev. B **40**, 6442 (1989).
[25] G. Manzke, K. Henneberger, and V. May, Phys. Status Solidi B **130**, 233 (1987).
[26] S. Schmitt-Rink, D. S. Chemla, and D. A. B. Miller, Phys. Rev. B **32**, 6601 (1985).